Theoretical and experimental study of a novel triple-magnet magnetic dynamic vibration absorber with tunable stiffness

Xiaoyu Chen and Yonggang Leng
School of Mechanical Engineering, Tianjin University, Tianjin, China
Fei Sun
School of Foreign Languages, Tianjin University, Tianjin, China, and
Xukun Su, Shuailing Sun and Junjie Xu
School of Mechanical Engineering, Tianjin University, Tianjin, China

Received 16 April 2023
Revised 11 May 2023
Accepted 18 May 2023

Abstract

Purpose – The existing Nonlinear Dynamic Vibration Absorbers (NLDVAs) have the disadvantages of complex structure, high cost, high installation space requirements and difficulty in miniaturization. And most of the NLDVAs have not been applied to reality. To address the above issues, a novel Triple-magnet Magnetic Dynamic Vibration Absorber (TMDVA) with tunable stiffness, only composed of triple cylindrical permanent magnets and an acrylic tube, is designed, modeled and tested in this paper.

Design/methodology/approach – (1) A novel TMDVA is designed. (2) Theoretical and experimental methods. (3) Equivalent dynamics model.

Findings – It is found that adjusting the magnet distance can effectively optimize the vibration reduction effect of the TMDVA under different resonance conditions. When the resonance frequency of the cantilever changes, the magnet distance of the TMDVA with a high vibration reduction effect shows an approximately linear relationship with the resonance frequency of the cantilever which is convenient for the design optimization of the TMDVA.

Originality/value – Both the simulation and experimental results prove that the TMDVA can effectively reduce the vibration of the cantilever even if the resonance frequency of the cantilever changes, which shows

Funding: This work is supported by the National Natural Science Foundation of China (Grant No. 52275122) and the National Natural Science Foundation of China (Grant No. 12132010).

Author contributions: All authors contributed to the study conception and design. Material preparation, data collection and analysis were performed by Xiaoyu Chen and Yonggang Leng. The experimental structures were made and prepared by Xiaoyu Chen. Fei Sun, Xukun Su, Shuailing Sun and Junjie Xu revised and polished the English writing of the manuscript. All authors read and approved the final manuscript.

Data availability: The data that support the findings of this study are available from the corresponding author upon reasonable request.

Competing interests: We declare that we have no financial and personal relationships with other people or organizations that can inappropriately influence our work, there is no professional or other personal interest of any nature or kind in any product, service and/or company that could be construed as influencing the position presented in, or the review of, the manuscript entitled, "Theoretical and Experimental Study of a Novel Triple-magnet Magnetic Dynamic Vibration Absorber With Tunable Stiffness".

Journal of Intelligent Manufacturing and Special Equipment
Vol. 4 No. 2, 2023
pp. 99-128
Emerald Publishing Limited
e-ISSN: 2633-660X
p-ISSN: 2633-6596
DOI 10.1108/JIMSE-04-2023-0002

the strong robustness of the TMDVA. Given all that, the TMDVA has potential application value in the passive vibration reduction of engineering structures.

Keywords Triple-magnet magnetic dynamic vibration absorber, Tunable stiffness, Nonlinear magnetic force, Magnet distance, Transient dynamics, Energy

Paper type Research paper

1. Introduction

Structural vibration is ubiquitous in various fields such as aerospace, mechanical and civil engineering. John Milne first proposed the concept of vibration control in the early 19th century (Housner *et al.*, 1997), and then Yao (1972) introduced it into civil engineering in 1972 to study the vibration control of civil structures. Dynamic Vibration Absorber (DVA), a kind of passive vibration reduction device, was first proposed by Frahm in 1909 (Xu, 2015). Till now, DVAs have been widely used in the vibration control of engineering structures. Linear Dynamic Vibration Absorber (LDVA), also called Tuned Mass Damper (TMD), is usually composed of a linear stiffness element, a mass block and a damping element. When the resonance frequency of the LDVA is approximately equal to the vibration frequency of the primary structure, the LDVA can provide the primary structure with a force that is opposite to the excitation force and can dissipate vibration energy through its damping (Liu *et al.*, 2007). The TMD classical design theory proposed by Den Hartog (1947) and Ormondroyd and Den Hartog (1928) has been widely used in the parameter optimization of TMDs or LDVAs. Cheng *et al.* (2020) have proposed a novel Inertial Amplification Mechanism (IAM) to improve the damping performance of a classical TMD. With IAM-TMD, the dynamic response of the primary structure and the damper are simultaneously mitigated. Christie *et al.* (2019) have developed a magnetorheological-fluid-based pendulum TMD, which is effective in reducing the dynamic response of multistory structures. Di Matte *et al.* (2019) have investigated the use of a TMD to control the response of foundation vibration isolation structures under random excitation. With proper optimization of the proposed procedure, the TMD can effectively reduce the response of the foundation isolation structure even under strong earthquakes. Bae *et al.* (2012) have proposed a new TMD consisting of a classical TMD and eddy current damping. The main advantages of this TMD are as follows: (1) it is relatively simple to apply; (2) it does not require any electronic equipment or external power supply; (3) it can effectively suppress the vibration of the primary structure. In all, the theory and research of TMDs have been developed over time. However, due to the narrowband vibration reduction performance and poor robustness of TMDs, it is difficult for TMDs to meet the vibration reduction requirements under complex working conditions.

With the development of the DVA research, increasing researchers begin to focus on the Nonlinear Dynamic Vibration Absorber (NLDVA). Roberson (1952) has indicated that introducing nonlinear stiffness to DVAs is beneficial to expanding the vibration reduction frequency band and enhancing the robustness of DVAs. There are many kinds of NLDVAs, such as cubic stiffness NLDVAs (Oueini *et al.*, 1999), piecewise stiffness NLDVAs (Pun and Liu, 2000) and tuned stiffness NLDVAs (Walsh and Lamancusa, 1992). Nonlinear Energy Sink (NES) is a kind of NLDVA that can make the vibration energy targeted transferred to itself from the primary structure and dissipated by the damping of the NES. NES has been first proposed and named by Vakakis (2001). And the NES enjoys the following characteristics: high energy dissipation efficiency, strong robustness, low mass and insensitivity to stiffness degradation (Zhang *et al.*, 2019; Gourdon *et al.*, 2007; Tripathi *et al.*, 2017; Guo *et al.*, 2015). Thanks to its strong nonlinear stiffness, the NES has no definite initial resonance frequency and can form an infinite number of nonlinear resonance conditions with different primary structures. Therefore, compared to TMDs, NESs have a wider vibration reduction frequency band. Javidialesaadi and Wierschem (2019) have introduced a new NES equipped with an inertial apparatus for passive vibration control of the primary structure and given results

related to the performance evaluation of the vibration reduction device. Geng *et al.* (2021) have proposed a new type of NES with limited vibration amplitude. Adjusting the design parameters of the NES appropriately can effectively reduce the dynamic response of the primary structure, which lays a foundation for the engineering application of the NES. Yao *et al.* (2019) have designed a grounded NES with segmental linear stiffness for the vibration reduction needs of modern rotating machinery. Simulation results show that the vibration reduction effect of this NES can reach 78%. According to the above references, it is found that the existing NESs have the disadvantages of complex structure, high cost and difficulty in miniaturization. And most of the NLDVAs have not been applied to reality.

In the studies of NLDVAs, the researchers have also paid attention to the DVA with magnetic properties. The nonlinear stiffness of the magnetic DVA is generated by the interaction between magnets (Zhang and Leng, 2020; Zhang *et al.*, 2017, 2020). Compared with NLDVAs constructed from nonmagnetic components, magnetic DVAs greatly reduce the difficulty of obtaining nonlinear stiffness. Moreover, magnetic DVAs are not prone to stiffness degradation because there is no contact between the magnets; therefore, they enjoy stronger stability and longer service life. Pennisi *et al.* (2018) have implemented the design of an NES with both positive and negative stiffness using some cylindrical permanent magnets and stored the vibration energy through the coil while damping. Benacchio *et al.* (2016) and Lo Feudo *et al.* (2019) have designed a magnetic DVA with tunable stiffness using some ring magnet sets and applied it to vibration control of a multistory structure. Chen *et al.* (2020) have used some rectangular magnets to design a bistable magnetic DVA suitable for vibration control of a multistory structure. Overall, the existing magnetic DVAs usually need a lot of magnets, which makes the structures of the magnetic DVAs complicated. Meanwhile, because of that, the magnetic DVAs, with high installation space requirements, are not conducive to miniaturization. It is difficult for the existing magnetic DVAs to be applied to the vibration reduction of small-sized structures.

Based on the above background and our preliminary work (Chen *et al.*, 2023a, b, c), a novel Triple-magnet Magnetic Dynamic Vibration Absorber (TMDVA) with tunable stiffness is designed, modeled and tested in this paper. The tuning methodology is passive, and it relies on the magnet distance of the TMDVA. The TMDVA is composed of only an acrylic tube and triple cylindrical permanent magnets. Its structure is simpler than that of other existing magnetic DVAs. The TMDVA creates a nonlinear magnetic force with the mutual repulsion between the triple magnets. Due to that, the stiffness characteristics of the nonlinear magnetic force can be changed when the magnet distance of the TMDVA is adjusted. No magnetic DVA with this kind of structural characteristic has been reported so far. A cantilever is taken as the vibration reduction object. And the theoretical model of the TMDVA cantilever vibration reduction system is established. Based on the equivalent magnetizing current theory, a calculation model of the nonlinear magnetic force is derived. Next, the influence of the magnet distance on the nonlinear stiffness characteristics is analyzed. Subsequently, the effect of the magnet distance (nonlinear stiffness characteristics) on the vibration reduction performance of the TMDVA is investigated from the perspective of transient dynamics and energy. After that, experiments are carried out to verify the correctness of the simulation results. Finally, the conclusions are drawn.

2. Theoretical model

2.1 Triple-magnet magnetic dynamic vibration absorber (TMDVA) cantilever vibration reduction system

Figure 1(a) is the schematic diagram of the TMDVA. The TMDVA is composed of triple cylindrical permanent magnets A, B and C and an acrylic tube D. The magnets A and C are fixedly connected to the tube D, and the positions of the two fixed magnets are adjustable. The magnet B repels not only the magnet A but also the magnet C, and can move inside the

tube D (the magnetic pole arrangements are shown in Figure 1(a)). l is the distance between the two fixed magnets A and C (from the upper surface of the magnet A to the lower surface of the magnet C). The stiffness of the nonlinear magnetic force can be changed when the magnet distance l is adjusted. s is the distance between the magnet A and the magnet B (from the upper surface of the magnet A to the lower surface of the magnet B). When the magnet B is excited to move, s changes accordingly. A cantilever is taken as the vibration reduction object. Figure 1(b) displays the schematic diagram of the TMDVA cantilever vibration reduction system. The free end of the cantilever E has a gripper G (considered as a mass block), and the TMDVA can be fixed with the cantilever through the gripper. The fixed end of the cantilever is fixed with a base F, which can be excited by an external excitation acceleration a. The direction of the acceleration is along the horizontal z-axis (the x-axis is perpendicular to the ground). l_E is the length of the cantilever when the cantilever remains stationary. Adjusting the length l_E can change the resonance frequency of the cantilever. z_c and z_m are displacements of the cantilever and the magnet B relative to the base F, respectively.

Figure 1(c) shows the equivalent dynamics model of the vibration reduction system. According to Newton's second law, the dynamics equations of the system can be written as follows:

$$\begin{cases} -k_1 z_c - c_1 \dot{z}_c + F_m - c_2(\dot{z}_c - \dot{z}_m) + m_1 a = m_1 \ddot{z}_c \\ -F_m - c_2(\dot{z}_m - \dot{z}_c) = m_2 \ddot{z}_m \end{cases} \tag{1}$$

In Equation (1), k_1 and c_1 are the equivalent stiffness coefficient and the equivalent damping coefficient of the cantilever, respectively. F_m is the nonlinear magnetic force on the cantilever. c_2 is the equivalent damping coefficient of the TMDVA, and m_2 is the mass of the magnet B. According to ref. Priya *et al.* (2010), k_1 and c_1 can be calculated using the following formulas:

$$k_1 = \frac{3EI}{{l_E}^3} \tag{2}$$

$$I = \frac{w_E {t_E}^3}{12} \tag{3}$$

$$c_1 = 2m_1 \xi_r \omega_r \tag{4}$$

$$\omega_r = \sqrt{\frac{k_1}{m_1}} \tag{5}$$

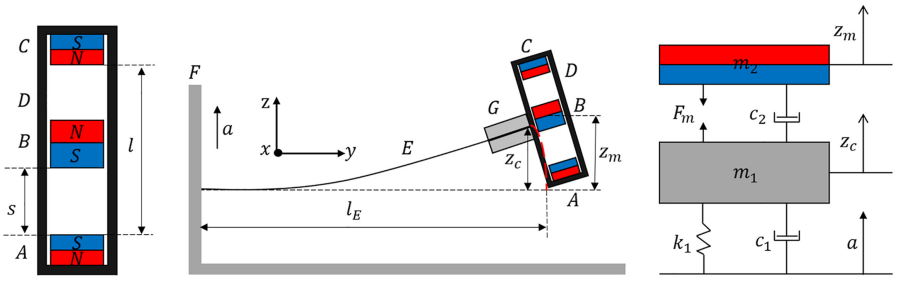

(a) (b) (c)

Figure 1.
(a) Schematic diagram of the TMDVA.
(b) Schematic diagram of the TMDVA cantilever vibration reduction system.
(c) The equivalent dynamics model of the TMDVA cantilever vibration reduction system

Source(s): Authors' own work

In Formula (2), E is the Young's modulus of the cantilever material. I is the equivalent section moment of inertia of the cantilever. In Formula (3), w_E and t_E are the width and thickness of the cantilever, respectively. In Formula (4), ξ_r is the equivalent damping ratio of the cantilever. ω_r is the natural frequency of the cantilever system. It is worth noting that the two fixed magnets, the gripper G and the tube D cannot move relative to the cantilever. Thus, m_1 should be calculated as follows:

$$m_1 = m_c + m_t + m_{fm} + m_G \tag{6}$$

$$m_c = \frac{33m_E}{140} \tag{7}$$

$$m_E = \rho l_E w_E t_E \tag{8}$$

In Formula (6), m_c is the equivalent mass of the cantilever. m_t is the mass of the tube D. m_{fm} is the mass of the magnets A and C. m_G is the mass of the gripper G. m_c can be calculated using Formulas (7) and (8). In Formula (8), ρ is the density of the cantilever. Based on the above, the vibration reduction effect of the TMDVA should be evaluated in comparison with an equivalent linear cantilever without the magnet B shown in Figure 2(a). Figure 2(b) depicts the equivalent dynamics model of the equivalent linear cantilever. Hence, the dynamics equation of the linear cantilever can be expressed as follows:

$$-k_1 z_l - c_1 \dot{z}_l + m_1 a = m_1 \ddot{z}_l \tag{9}$$

In Formula (9), z_l is the linear cantilever displacement relative to the base F. The other parameters have the same meaning as those in Equation (1).

In the real case, the magnet B is also affected by friction damping (coulomb damping). Therefore, the dynamics Equation (1) needs to be modified:

$$\begin{cases} -k_1 z_c - c_1 \dot{z}_c + F_m - c_2(\dot{z}_c - \dot{z}_m) + m_1 a + \mu m_2 g \cdot sgn(\dot{z}_m - \dot{z}_c) = m_1 \ddot{z}_c \\ -F_m - c_2(\dot{z}_m - \dot{z}_c) - \mu m_2 g \cdot sgn(\dot{z}_m - \dot{z}_c) = m_2 \ddot{z}_m \end{cases} \tag{10}$$

In Formula (10), μ is the friction coefficient. g is the gravitational acceleration and its value is 9.8 m/s^2. $sgn(\dot{z}_m - \dot{z}_c)$ is the sign function, which is given by

$$sgn(\dot{z}_m - \dot{z}_c) = \begin{cases} -1, \dot{z}_m - \dot{z}_c \le 0 \\ 1, \dot{z}_m - \dot{z}_c > 0 \end{cases} \tag{11}$$

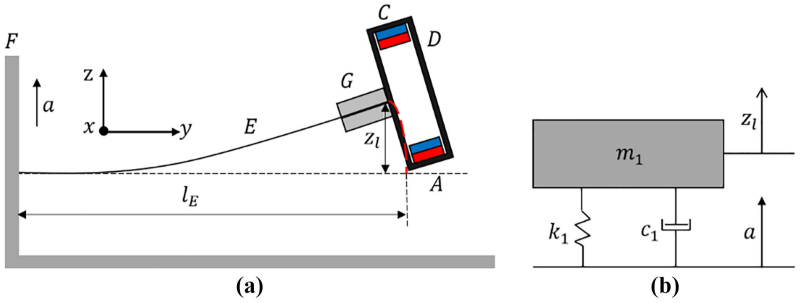

(a) (b)

Source(s): Authors' own work

Figure 2.
(a) Equivalent linear cantilever (without the magnet B). (b) Equivalent dynamics model of the equivalent linear cantilever

2.2 Nonlinear magnetic force

2.2.1 Theoretical model. The calculation model of the nonlinear magnetic force F_m is established based on the equivalent magnetizing current theory (Zhang and Leng, 2020; Zhang *et al.*, 2017, 2020). For an axially magnetized cylindrical permanent magnet, the distribution of surface equivalent magnetization current is circular around the magnetization axis. The coordinate system is established by taking the center of the circle current as the original point shown in Figure 3. The following relations can be achieved:

$$\boldsymbol{R} = x\boldsymbol{i} + y\boldsymbol{j} + z\boldsymbol{k} \tag{12}$$

$$\boldsymbol{l} = l\cos\theta\boldsymbol{i} + l\sin\theta\boldsymbol{j}, d\boldsymbol{l} = -l\sin\theta d\theta\boldsymbol{i} + l\cos\theta d\theta\boldsymbol{j} \tag{13}$$

$$\boldsymbol{r} = \boldsymbol{R} - \boldsymbol{l} = (x - l\cos\theta)\boldsymbol{i} + (y - l\sin\theta)\boldsymbol{j} + z\boldsymbol{k} \tag{14}$$

$$d\boldsymbol{l} \times \boldsymbol{r} = zl\cos\theta d\theta\boldsymbol{i} + zl\sin\theta d\theta\boldsymbol{j} + l(l - x\cos\theta - y\sin\theta)d\theta\boldsymbol{k} \tag{15}$$

Magnetic induction intensity generated by a permanent magnet in space can be calculated according to Biot Savart's Law. The magnetic induction intensity generated by a section of the current element at an arbitrary point P in space can be expressed as follows:

$$\boldsymbol{B} = \int_L \frac{\mu_0 I}{4\pi} \frac{d\boldsymbol{l} \times \boldsymbol{r}}{r^3} \tag{16}$$

In Formula (16), $\boldsymbol{B}$ is the magnetic induction intensity generated by a permanent magnet. L is the integral path of the current. μ_0 is the space permeability. I can be expressed as follows:

$$I = \int_t K_m dt \tag{17}$$

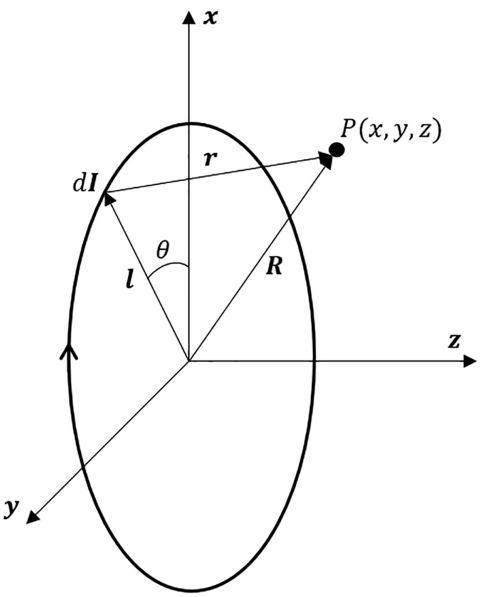

Source(s): Authors'own work

Figure 3.
Coordinate system of the magnetic field produced by a circular current loop

t represents the width of the current. K_m is the surface magnetizing current density, the formula of which is

$$\boldsymbol{K_m} = \boldsymbol{M} \times \hat{\boldsymbol{n}} \tag{18}$$

where $\boldsymbol{M}$ is the magnetization intensity of the permanent magnet and $\hat{\boldsymbol{n}}$ is the surface normal unit vector. Subsequently, the origin of the coordinate system is moved to the geometric center of cylindrical magnet A. In Figure 4, the magnetic induction intensity at an arbitrary point produced by cylindrical magnet A can be derived as follows:

$$\begin{aligned}\boldsymbol{B} = &\frac{\mu_0 M_A}{4\pi}\int_{-\frac{l_A}{2}}^{\frac{l_A}{2}} dz_1 \int_0^{2\pi} \frac{(z-z_1)r_A\cos\theta}{r^3} d\theta \boldsymbol{i} + \frac{(z-z_1)r_A\sin\theta}{r^3} d\theta \boldsymbol{j} \\ &+\frac{\mu_0 M_A}{4\pi}\int_{-\frac{l_A}{2}}^{\frac{l_A}{2}} dz_1 \int_0^{2\pi} \frac{r_A(r_A - x\cos\theta - y\sin\theta)}{r^3} d\theta \boldsymbol{k}\end{aligned} \tag{19}$$

In Equation (19), $r = \left((x - r_A\cos\theta)^2 + (y - r_A\sin\theta)^2 - (z - z_1)^2\right)^{1/2}$. l_A and r_A are the height and radius of the magnet A, respectively. M_A is the magnetization of the magnet A. Let $\boldsymbol{i}$, $\boldsymbol{j}$ and $\boldsymbol{k}$ be the unit vectors in the x, y and z directions, respectively. The magnetic induction $\boldsymbol{B}$ is represented as a vector:

$$\boldsymbol{B} = B_i\boldsymbol{i} + B_j\boldsymbol{j} + B_k\boldsymbol{k} \tag{20}$$

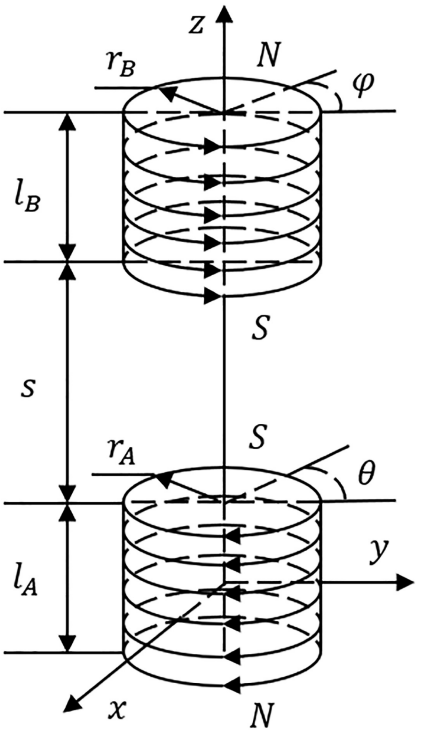

Source(s): Authors' own work

Figure 4.
The positions of magnetizing currents on the surface of cylindrical magnets in the coordinate system

According to Ampere's law, the interacting magnetic force $\boldsymbol{F}$ between the two cylindrical permanent magnets A and B is derived as follows:

$$\boldsymbol{F} = \iint_S \boldsymbol{K_{mB}} \times \boldsymbol{B} dS = \iint_S \begin{vmatrix} \boldsymbol{i} & \boldsymbol{j} & \boldsymbol{k} \\ -M_B \sin\varphi & M_B \cos\varphi & 0 \\ B_i & B_j & B_k \end{vmatrix} dz_2 r_B d\varphi \tag{21}$$

After calculation, $\boldsymbol{F}$ can be written as follows:

$$\begin{aligned} \boldsymbol{F} = {} & M_B \int_{-\frac{l_B}{2}}^{\frac{l_B}{2}} dz_2 \int_0^{2\pi} B_k(x + r_B cos\,\varphi, y + r_B sin\,\varphi, z + z_2) cos\,\varphi r_B d\varphi \boldsymbol{i} \\ & + M_B \int_{-\frac{l_B}{2}}^{\frac{l_B}{2}} dz_2 \int_0^{2\pi} B_k(x + r_B cos\,\varphi, y + r_B sin\,\varphi, z + z_2) sin\,\varphi r_B d\varphi \boldsymbol{j} \\ & - M_B \int_{-\frac{l_B}{2}}^{\frac{l_B}{2}} dz_2 \int_0^{2\pi} B_i(x + r_B cos\,\varphi, y + r_B sin\,\varphi, z + z_2) cos\,\varphi r_B d\varphi \boldsymbol{k} \\ & - M_B \int_{-\frac{l_B}{2}}^{\frac{l_B}{2}} dz_2 \int_0^{2\pi} B_j(x + r_B cos\,\varphi, y + r_B sin\,\varphi, z + z_2) sin\,\varphi r_B d\varphi \boldsymbol{k} \end{aligned} \tag{22}$$

In Formula (22), $z = s + \frac{l_A}{2} + \frac{l_B}{2}$. l_B and r_B are the height and radius of the magnet B. M_B is the magnetization of the magnet B. F_m in dynamics Equations (1) and (10) is the nonlinear magnetic force acting on the cantilever. According to Newton's third law and Formula (22), the nonlinear magnetic force F_m is derived as follows:

$$\begin{aligned} F_m = {} & M_B \int_{-\frac{l_B}{2}}^{\frac{l_B}{2}} dz_2 \int_0^{2\pi} B_i(x + r_B cos\,\varphi, y + r_B sin\,\varphi, z_a + z_2) cos\,\varphi r_B d\varphi \\ & + M_B \int_{-\frac{l_B}{2}}^{\frac{l_B}{2}} dz_2 \int_0^{2\pi} B_j(x + r_B cos\,\varphi, y + r_B sin\,\varphi, z_a + z_2) sin\,\varphi r_B d\varphi \\ & - M_B \int_{-\frac{l_B}{2}}^{\frac{l_B}{2}} dz_2 \int_0^{2\pi} B_i(x + r_B cos\,\varphi, y + r_B sin\,\varphi, z_b + z_2) cos\,\varphi r_B d\varphi \\ & - M_B \int_{-\frac{l_B}{2}}^{\frac{l_B}{2}} dz_2 \int_0^{2\pi} B_j(x + r_B cos\,\varphi, y + r_B sin\,\varphi, z_b + z_2) sin\,\varphi r_B d\varphi \end{aligned} \tag{23}$$

where $z_a = s + \frac{l_A}{2} + \frac{l_B}{2}$, $z_b = l - s + \frac{l_A}{2} + \frac{l_B}{2}$. The relationship among s, z_c and z_m is given by

$$s = \frac{l - l_B}{2} - (z_m - z_c) \tag{24}$$

2.2.2 Nonlinear magnetic force and stiffness characteristics. The parameters of the magnets are shown in Table A1 of Appendix. Figure 5(a) shows the nonlinear magnetic force F_m when the magnet distance l changes. The figure indicates that changing the magnet distance l can

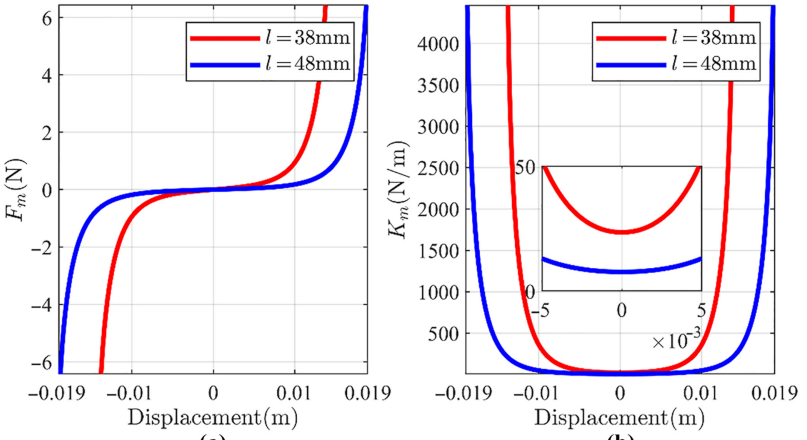

Source(s): Authors'own work

Figure 5. Theoretical results of (a) the nonlinear magnetic force F_m and (b) the magnetic stiffness K_m when the magnet distance changes

obviously affect the characteristics of the magnetic force. Figure 5(b) depicts the diagram of the magnetic stiffness. The minimum stiffness of the magnetic force appears at the displacement origin. In the figure, when the magnet distance l is 38 mm, the minimum stiffness value of the magnetic force is 23.63 N/m. And when l is 48 mm, the minimum stiffness value is 7.72 N/m. The larger the magnet distance l, the smaller the minimum stiffness value. Furthermore, the overall magnetic stiffness when $l = 38$ mm is larger than that when $l = 48$ mm. The magnetic stiffness curve of $l = 38$ mm changes more drastically and its magnetic force exhibits stronger nonlinear characteristics. Therefore, decreasing the magnet distance can not only increase the minimum magnetic stiffness value of the nonlinear magnetic force but also make the magnetic stiffness near the displacement origin change more drastically.

To further understand the characteristics of the nonlinear magnetic force F_m and the magnetic stiffness, the polynomial fitting formula of the force F_m is given by

$$\begin{aligned} F_m = {} & K_9(z_m - z_c)^9 + K_7(z_m - z_c)^7 \\ & + K_5(z_m - z_c)^5 \\ & + K_3(z_m - z_c)^3 + K_1(z_m - z_c) \end{aligned} \tag{25}$$

In Formula (25), $K_1, \cdots K_9$ are the stiffness coefficients. For example, when the magnet distances are 38 and 48 mm, respectively, the nonlinear magnetic force fitting formulas are shown in Formulas (26) and (27), respectively. The Root Mean Square Error (RMSE) is less than 2%.

$$\begin{aligned} F_{m38} \approx {} & 1.069 \times 10^{18} \times (z_m - z_c)^9 - 2.967 \times 10^{14} \times (z_m - z_c)^7 \\ & + 3.432 \times 10^{10} \times (z_m - z_c)^5 \\ & - 9.464 \times 10^5 \times (z_m - z_c)^3 + 36.3 \times (z_m - z_c) \end{aligned} \tag{26}$$

$$\begin{aligned} F_{m48} \approx {} & 1.026 \times 10^{17} \times (z_m - z_c)^9 - 5.506 \times 10^{13} \times (z_m - z_c)^7 \\ & + 1.113 \times 10^{10} \times (z_m - z_c)^5 \\ & - 7.133 \times 10^5 \times (z_m - z_c)^3 + 22.3 \times (z_m - z_c) \end{aligned} \tag{27}$$

Figure 6 shows the variation of the stiffness coefficients in the nonlinear magnetic force fitting formula when the magnet distance l changes. From the figure, as the magnet distance l increases, K_9, K_5 and K_1 all decrease significantly. K_7 increases gradually with the increase of

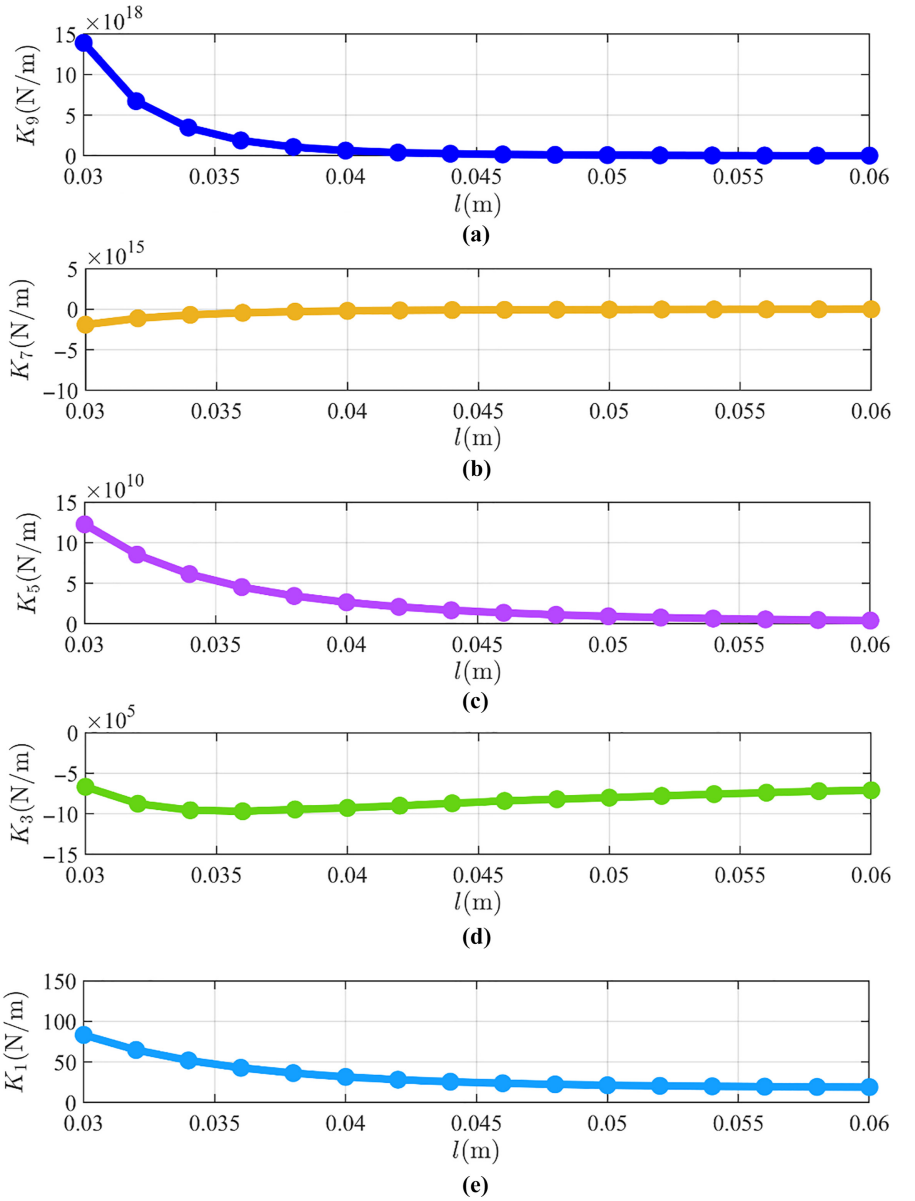

Source(s): Authors' own work

Figure 6.
The variations of the stiffness coefficients in the fitting formula with the change of the magnet distance l

the magnet distance l, while K_3 decreases first and subsequently increases. Compared with the three stiffness coefficients K_9, K_5 and K_1, the variations of the coefficients K_7 and K_3 are much smaller. This illustrates that the magnet distance mainly affects the characteristics of the nonlinear magnetic force through K_9, K_5 and K_1. Therefore, as the magnet distance increases, the stiffness of the magnetic force (in the same displacement interval) will decrease overall.

In Figure 6, when the magnet distance is approximately less than 40 mm, the stiffness coefficients in the magnetic force fitting formula exhibit large variations with the change of the magnet distance. On the contrary, when the magnet distance is approximately larger than 40 mm, the variations of the stiffness coefficients become very small as the magnet distance changes. This indicates that when the magnet distance is small, the adjustment of the magnet distance has a significant effect on the characteristics of the nonlinear magnetic force. When the magnet distance is large, the influence of the magnet distance on the nonlinear magnetic force becomes smaller. From this, changing the magnet distance essentially affects the nonlinear magnetic stiffness. Hence, the change of the magnet distance means the adjustment of the TMDVA's stiffness.

3. Numerical simulation

In this section, from the perspective of transient dynamics and energy, the influence of the magnet distance change (the adjustment of the magnetic stiffness) on the TMDVA vibration reduction performance is revealed. The parameters of the TMDVA and the cantilever are shown in Table A2 of Appendix. For descriptive convenience, the TMDVA with a magnet distance of 38 mm is named TMDVA-38. And when the magnet distance of the TMDVA is 48 mm, the TMDVA is named TMDVA-48. The amplitude of the acceleration a is 8.7 g. And the dynamics equations are solved using the Runge–Kutta method.

To evaluate the vibration reduction effect of the TMDVA, the vibration reduction percentage RE, % is introduced as follows:

$$RE, \% = \frac{RMS(z_l) - RMS(z_c)}{RMS(z_l)} \times 100\% \tag{28}$$

$RMS(z_l)$ represents the root mean square of the linear cantilever displacement in a certain time regime. $RMS(z_c)$ represents the root mean square of the cantilever displacement after vibration reduction in the same time regime. The time regime is $0 \sim 12$s in this paper.

In order to reveal the energy transfer characteristics of the system, an energy index is introduced as follows:

$$E_{INS}, \% = \frac{T_{DVA} + V_{DVA}}{T_{CANT} + V_{CANT} + T_{DVA} + V_{DVA}} \times 100\% \tag{29}$$

E_{INS}, % represents the percentage of instantaneous total energy carried by the magnet B in the TMDVA. And

$$T_{CANT} = \frac{1}{2} m_1 \dot{z}_c^{\,2} \tag{30}$$

$$V_{CANT} = \frac{1}{2} k_1 z_c^{\,2} \tag{31}$$

$$T_{DVA} = \frac{1}{2} m_2 \dot{z}_m^{\,2} \tag{32}$$

$$V_{DVA} = \int F_m d(z_m - z_c) \tag{33}$$

In Formulas (30)~(33), T and V represent the kinetic energy and the potential energy, respectively. Formulas (30)~(31) correspond to the energy of the cantilever. Formulas (32)~(33) correspond to the energy of the TMDVA.

3.1 The length l_E of the cantilever is 92 mm

Figure 7 displays the time-domain waveform and the spectrum of the linear cantilever displacement response when the length l_E of the cantilever is 92 mm. Figure 7(a) shows that the linear cantilever system performs free vibration, and the vibration amplitude of the linear cantilever descends very slowly. Figure 7(b) indicates that the resonance frequency of the linear cantilever is about 16.7 Hz. Figure 8 depicts the displacement response time-domain waveforms of the TMDVA cantilever vibration reduction system and the displacement response time-domain waveforms of the magnet B. In Figure 8(a) and (c), the vibration

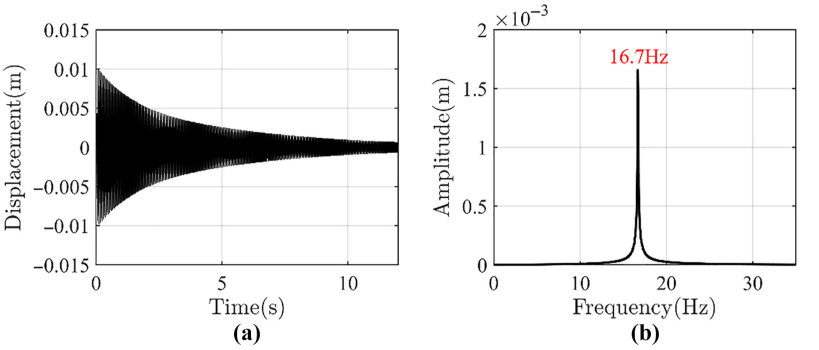

Figure 7.
(a) The displacement response time-domain waveform of the linear cantilever for l_E = 92 mm. (b) The spectrum of the linear cantilever for l_E = 92 mm

Source(s): Authors'own work

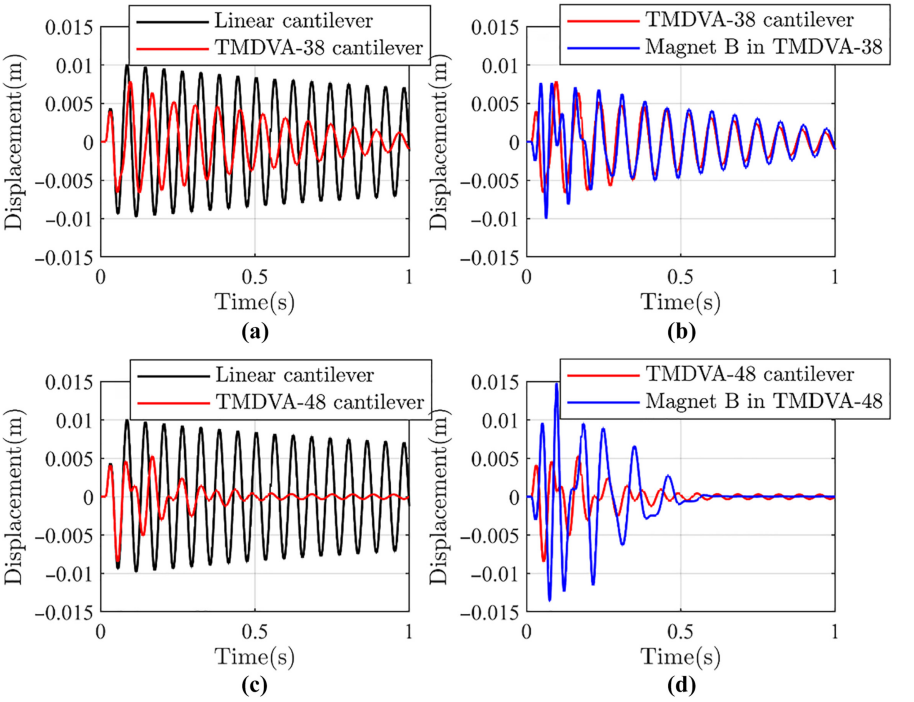

Figure 8.
The displacement response time-domain waveforms of (a) the linear cantilever and the TMDVA-38 cantilever, (b) the TMDVA-38 cantilever and the magnet B in the TMDVA-38, (c) the linear cantilever and the TMDVA-48 cantilever and (d) the TMDVA-48 cantilever and the magnet B in the TMDVA-48 when the resonance frequency of the linear cantilever is 16.7 Hz

Source(s): Authors'own work

reduction effect RE, % of the TMDVA-38 and the TMDVA-48 is 66.87% and 81.01%, respectively. The vibration reduction effect of the TMDVA-48 is better than that of the TMDVA-38 under this situation.

In Figure 8(b) and (d), the displacement of the magnet B is overall higher than that of the cantilever, which demonstrates the targeted transfer of vibration energy to the TMDVA. However, compared with the TMDVA-38 vibration reduction system, the trend of the energy transfer is more pronounced in the TMDVA-48 vibration reduction system, indicating that more energy is dissipated in the TMDVA-48. The percentage of instantaneous total energy carried by the magnet B depicted in Figure 9 illustrates that there are strong energy exchanges between the cantilever and the TMDVA in the initial time period. The characteristics of the energy transfer show that nonlinear beat phenomena occur in both the two vibration reduction systems. Another indication that the nonlinear beating occurs is that the envelope of the magnet B response undergoes large modulations in this case in Figure 8(b) and (d). Figure 9(a) illustrates that the nonlinear beat phenomenon dominates the early regime of the motion in the TMDVA-38 vibration reduction system. However, a less vigorous but faster energy exchange is now observed after 0.5s. Figure 8(b) demonstrates that 1:1 Transient Resonance Capture (1:1TRC) occurs in the TMDVA-38 system (Vakakis *et al.*, 2008). However, Figure 9(b) illustrates that the nonlinear beat phenomenon dominates the entire vibration reduction process of the TMDVA-48 system, and E_{INS}, % almost reaches 100%. That means the TMDVA-48 can dissipate more vibration energy in a short time. Due to that, the vibration reduction effect of the TMDVA-48 is better than that of the TMDVA-38.

Figure 10 shows the system Wavelet Transform (WT) spectra, which provide further evidence for the nonlinear beat phenomenon and 1:1 TRC. Figure 10(b) indicates that, in 0∼0.5s, 1:1 internal resonance and 2:1 super-harmonic resonance occurred in the TMDVA-38, which makes the nonlinear beat phenomenon dominate the motion of the system in that time regime. During this process, the 2:1 super-harmonic resonance gradually weakened, so that the nonlinear beat phenomenon of the system weakened until it completely disappeared after 0.5s, creating conditions for the 1:1 TRC. Figure 10(d) demonstrates that strong 1:1 internal resonance and 3:2 super-harmonic resonance appeared in the TMDVA-48, and the two resonances almost always appear at the same time. Therefore, the nonlinear beat phenomenon nearly dominates the entire vibration reduction process of the TMDVA-48.

3.2 The length l_E of the cantilever is 52 mm

Figure 11 displays the time-domain waveform and the spectrum of the linear cantilever displacement response when the length l_E of the cantilever is 52 mm. Figure 11(b) indicates

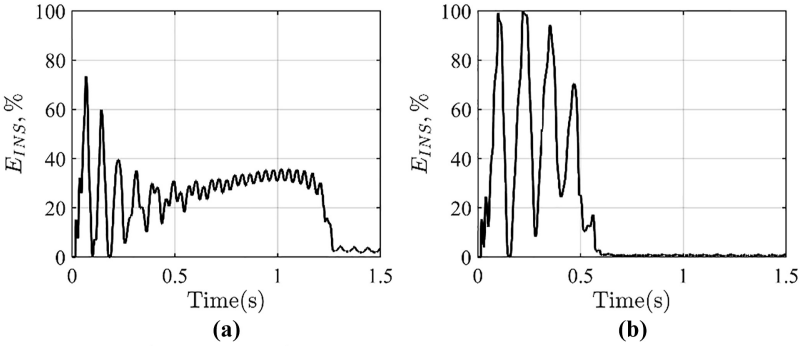

Source(s): Authors' own work

Figure 9.
The percentage of instantaneous total energy carried by the magnet B in the TMDVA when the resonance frequency of the linear cantilever is 16.7 Hz. (a) TMDVA-38. (b) TMDVA-48

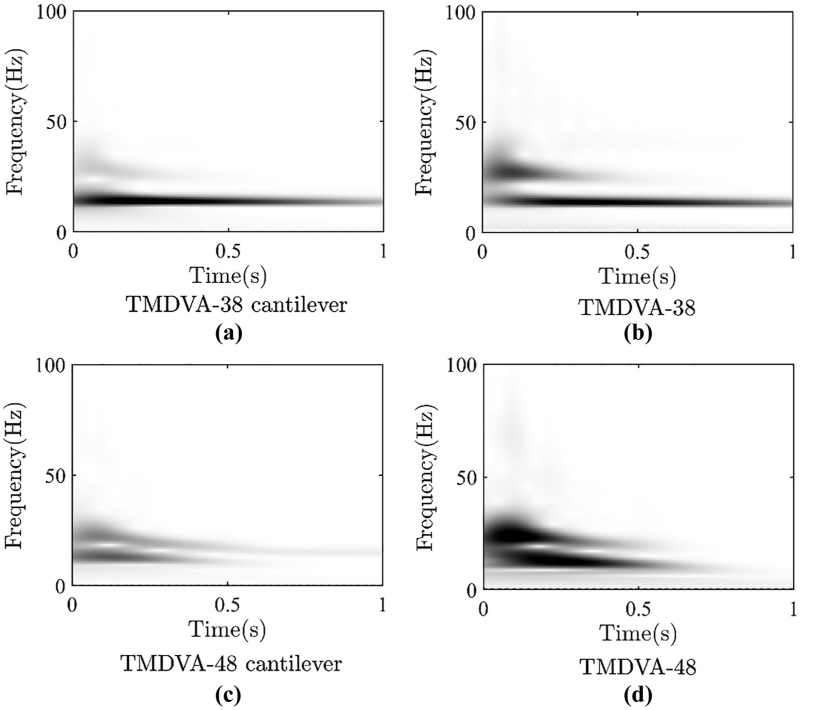

Figure 10.
The WT spectra of the TMDVA cantilever vibration reduction system displacement response when the resonance frequency of the linear cantilever is 16.7 Hz

Source(s): Authors' own work

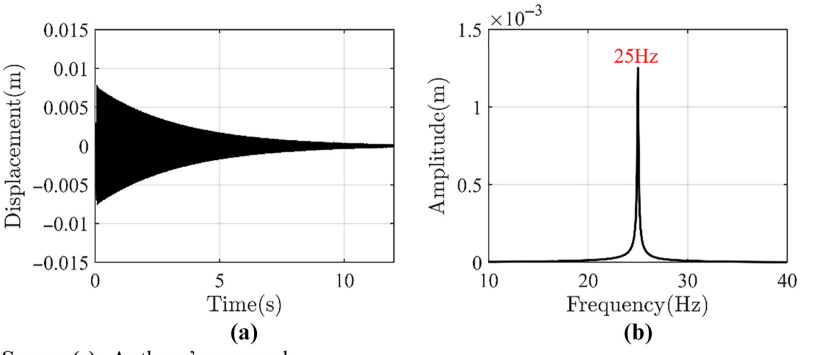

Figure 11.
(a) The displacement response time-domain waveform of the linear cantilever for $l_E = 52$ mm. (b) The spectrum of the linear cantilever for $l_E = 52$ mm

Source(s): Authors' own work

that the resonance frequency of the linear cantilever is approximately 25 Hz, which is higher than that in Section 3.1. Figure 12 depicts the displacement response time-domain waveforms of the TMDVA cantilever vibration reduction system. In Figure 12(a) and (c), the vibration reduction effect *RE*, % of the TMDVA-38 is 80.26% and the vibration reduction effect of the TMDVA-48 is 69.69%. The vibration reduction effect of the TMDVA-38 is better than that of the TMDVA-48, which is different from the condition when the length of the cantilever is 92 mm (the resonance frequency is 16.7 Hz).

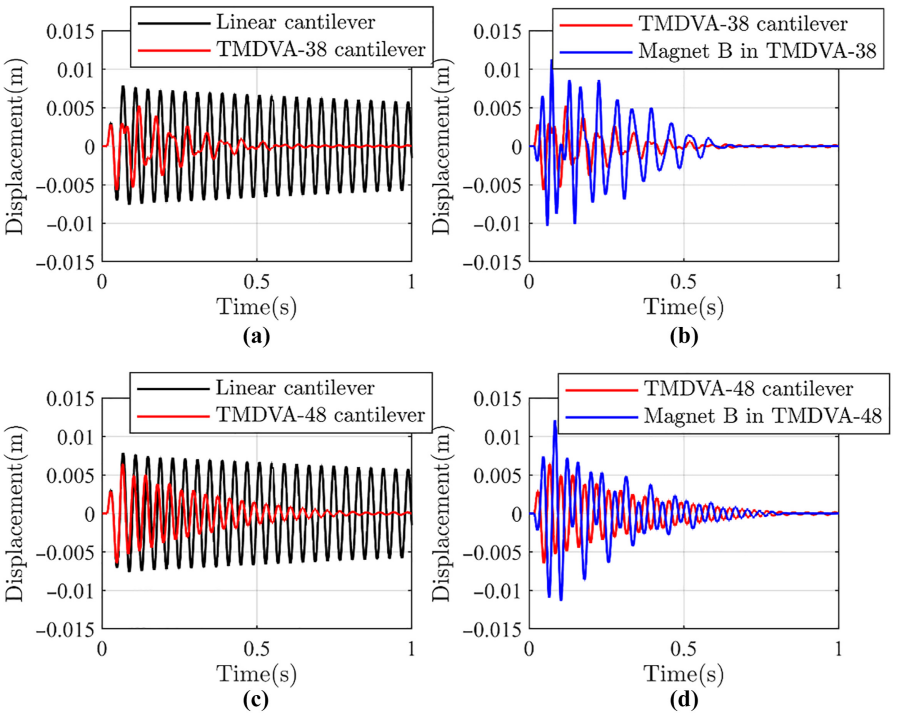

Source(s): Authors' own work

Figure 12. The displacement response time-domain waveforms of (a) the linear cantilever and the TMDVA-38 cantilever, (b) the TMDVA-38 cantilever and the magnet B in the TMDVA-38, (c) the linear cantilever and the TMDVA-48 cantilever and (d) the TMDVA-48 cantilever and the magnet B in the TMDVA-48 when the resonance frequency of the linear cantilever is 25 Hz

Figure 13 shows the percentage of instantaneous total energy carried by the magnet B in the TMDVA. From Figures 12 and 13(b) and (d), it can be seen that the vibration energy has also been targeted transferred to the TMDVA. In the TMDVA-38 vibration reduction system, a nonlinear beat phenomenon dominates the entire vibration reduction process. And the overall trend of E_{INS}, % rises as time goes by. On the contrary, the percentage of instantaneous total energy carried by the magnet B in the TMDVA-48 shown in Figure 13(b) illustrates that, although the energy exchange between the TMDVA-48 and the cantilever is fast, the

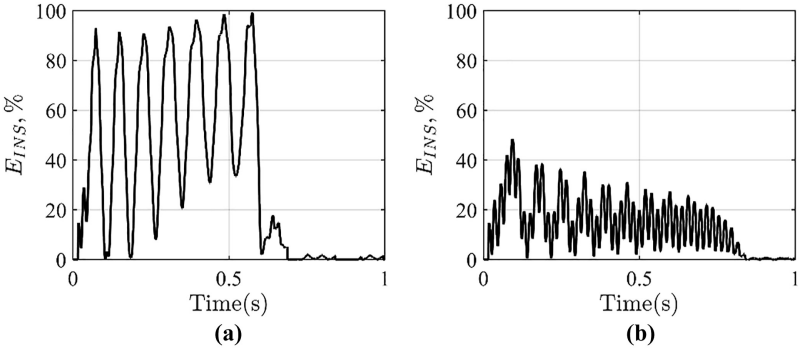

Source(s): Authors' own work

Figure 13. The percentage of instantaneous total energy carried by the magnet B in the TMDVA when the resonance frequency of the linear cantilever is 25 Hz. (a) TMDVA-38. (b) TMDVA-48

percentage of the energy carried by the magnet B in the TMDVA-48 never exceeds 50%. And the overall trend of E_{INS}, % gradually decreases with time. Because of these issues, the vibration reduction effect of the TMDVA-48 is worse than that of the TMDVA-38.

Figure 14 displays the system's WT spectra when the resonance frequency of the linear cantilever is 25 Hz. Figure 14(b) indicates that 1:1 internal resonance and 3:2 super-harmonic resonance appeared in the TMDVA-38. At the same time, some weak subharmonic

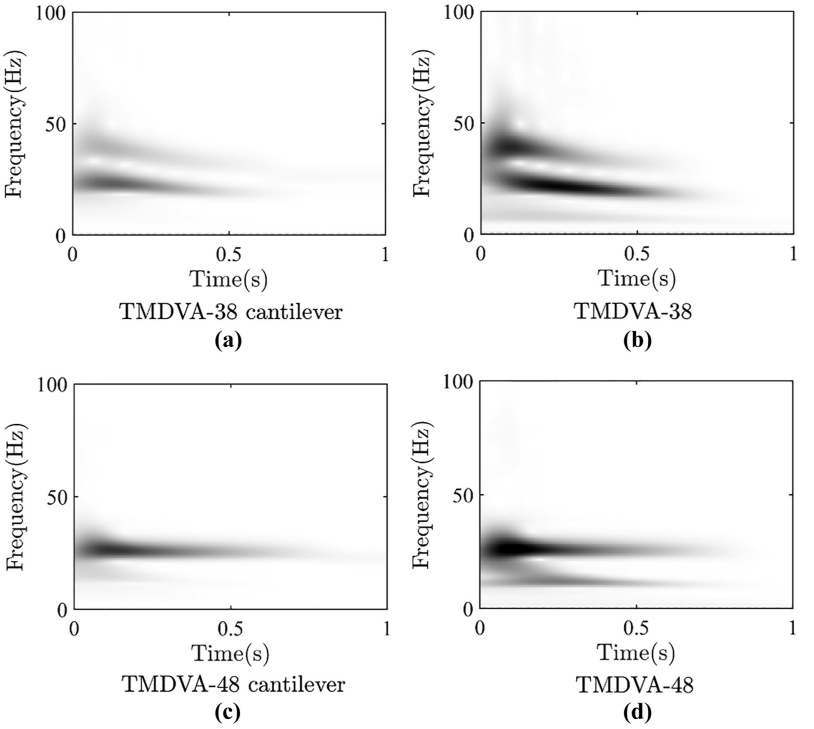

Figure 14.
The WT spectra of the TMDVA cantilever vibration reduction system displacement response when the resonance frequency of the linear cantilever is 25 Hz

Source(s): Authors' own work

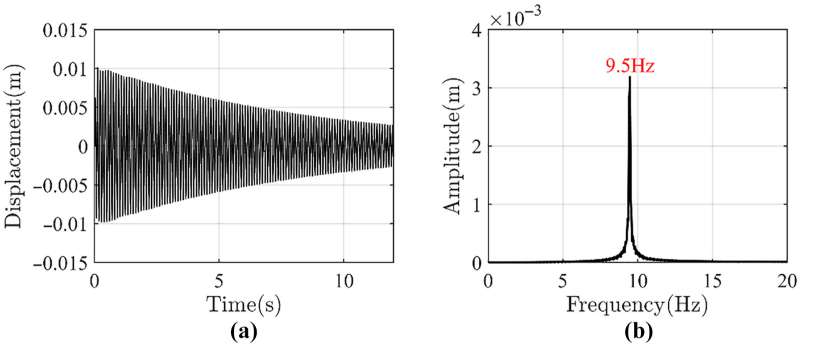

Figure 15.
(a) The displacement response time-domain waveform of the linear cantilever for l_E = 140 mm. (b) The spectrum of the linear cantilever for l_E = 140 mm

Source(s): Authors' own work

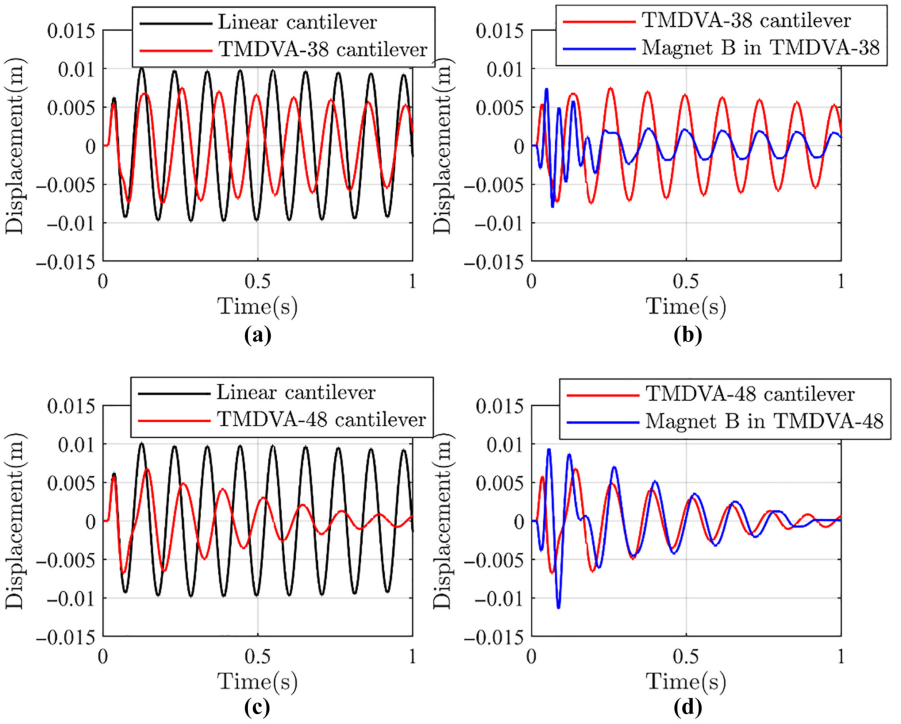

Source(s): Authors' own work

Figure 16. The displacement response time-domain waveforms of (a) the linear cantilever and the TMDVA-38 cantilever, (b) the TMDVA-38 cantilever and the magnet B in the TMDVA-38, (c) the linear cantilever and the TMDVA-48 cantilever and (d) the TMDVA-48 cantilever and the magnet B in the TMDVA-48 when the resonance frequency of the linear cantilever is 9.5 Hz

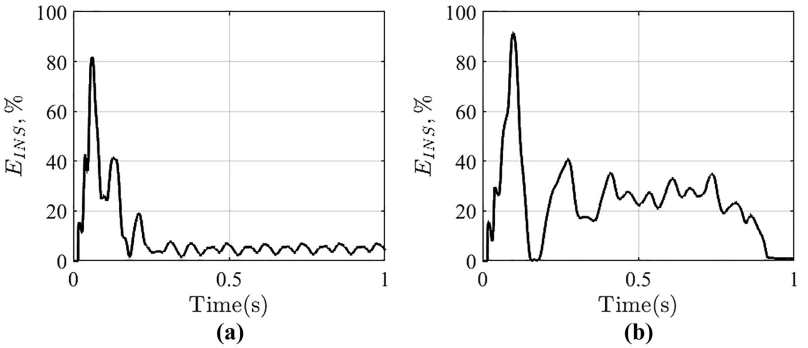

Source(s): Authors' own work

Figure 17. The percentage of instantaneous total energy carried by the magnet B in the TMDVA when the resonance frequency of the linear cantilever is 9.5 Hz. (a) TMDVA-38. (b) TMDVA-48

resonances also occur in the system. Figure 14(d) illustrates that 1:1 internal resonance and 1:2 subharmonic resonance occurred in the TMDVA-48. However, because the 1:2 subharmonic resonance is much weaker than the 1:1 internal resonance, the manners of energy transfer between the TMDVA-48 and the cantilever are mainly 1:1 internal resonance.

Through the analysis in Section 3.1 and this section, it can be found that the TMDVA can achieve resonance capture with cantilevers with different resonance frequencies. When the magnet distance of the TMDVA changes, the nonlinear magnetic stiffness changes

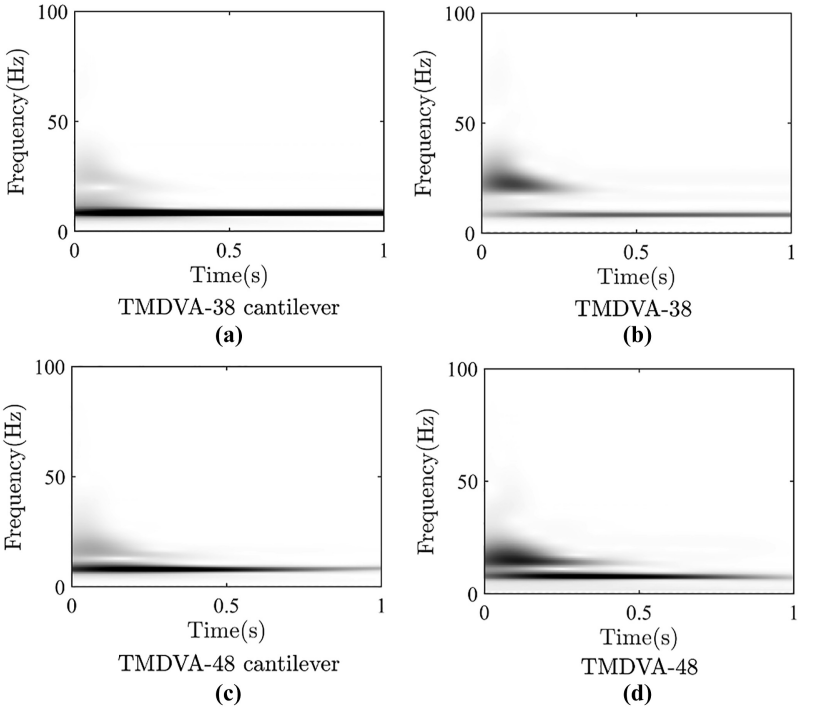

Figure 18.
The WT spectra of the TMDVA cantilever vibration reduction system displacement response when the resonance frequency of the linear cantilever is 9.5 Hz

Source(s): Authors' own work

accordingly. Due to this, the TMDVA-38 and the TMDVA-48 exhibit different vibration reduction performances. In general, the minimum magnetic stiffnesses of nonlinear magnetic forces corresponding to different magnet distances are different. For example, the minimum values of nonlinear magnetic stiffnesses with magnet distances of 38 mm and 48 mm are 23.63 N/m and 7.72 N/m, respectively. The nonlinear magnetic force with a magnet distance of 38 mm lacks stiffness components less than 23.63 N/m. And the nonlinear magnetic force with a magnet distance of 48 mm lacks stiffness components less than 7.72 N/m. The absence of low-stiffness components means that the TMDVA cannot form low-frequency resonance conditions with primary structures with lower resonance frequencies. Thus, when the resonance frequency of the primary structure is low, the TMDVA with a too small magnet distance, such as 38 mm, may not be able to achieve 1:1 resonance capture with the primary structure, resulting in a limited vibration reduction effect of the TMDVA. From this, for the primary structures with lower resonance frequencies, the TMDVA-48 may be able to show a better vibration reduction performance because of its larger magnet distance.

3.3 The length l_E of the cantilever is 140 mm

In order to verify the correctness of the analysis in Section 3.2, the length of the cantilever is adjusted to 140 mm. Figure 15 shows the time-domain waveform and the spectrum of the linear cantilever displacement response when the length l_E of the cantilever is 140 mm. Figure 15(b) indicates that the resonance frequency of the linear cantilever is approximately 9.5 Hz under this condition. Figure 16 depicts the displacement response time-domain waveforms of the TMDVA cantilever vibration reduction system when the resonance frequency of the linear cantilever is 9.5 Hz. In Figure 16(a) and (c), the vibration reduction

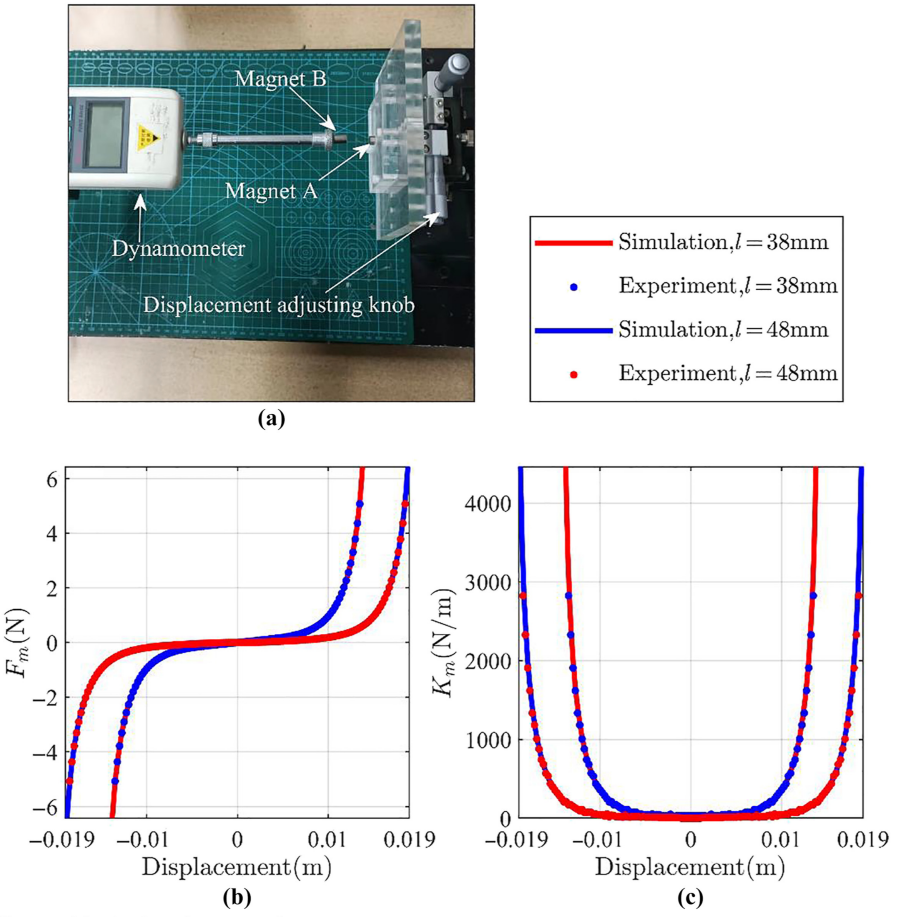

Source(s): Authors'own work

Figure 19. (a) Magnetic force measurement system. (b) Comparison of the experimental and theoretical results of the nonlinear magnetic force F_m. (c) Diagram of the variation of the magnetic force stiffness K_m

effect *RE*, % of the TMDVA-38 is 59.61%, and the vibration reduction effect *RE*, % of the TMDVA-48 is 80.68%. Figure 16(b) illustrates that the displacement amplitude of magnet B in TMDVA-38 is always much smaller than that of the cantilever after 0.2s. It means that the vibration energy of the system cannot be targeted transferred to the TMDVA-38 anymore after 0.2s. After 0.2s, E_{INS}, % is always kept around 5%, and most of the vibration energy in the system is stored in the cantilever. On the contrary, the TMDVA-48 still shows a good vibration reduction performance in this case (see Figure 17).

Figure 18 depicts the system's WT spectra when the resonance frequency of the linear cantilever is 9.5 Hz. Figure 18(b) shows that the manner of energy exchange between the TMDVA-38 and the cantilever in 0∼0.2s is mainly 3:1 super-harmonic resonance. The weak 1:1 internal resonance in the TMDVA-38 is almost negligible compared to the previous two cases (which are shown in Figures 10(b) and 14(b)). Significantly different from the TMDVA-38, Figure 18(d) indicates that the TMDVA-48 undergoes a strong 1:1 resonance capture with the cantilever. And the TMDVA-48 also undergoes 2:1 super-harmonic resonance in 0–0.5s. These pieces of evidence verify the correctness of the previous analysis. The nonlinear magnetic force of the TMDVA-38 lacks stiffness components less than 23.63 N/m, which

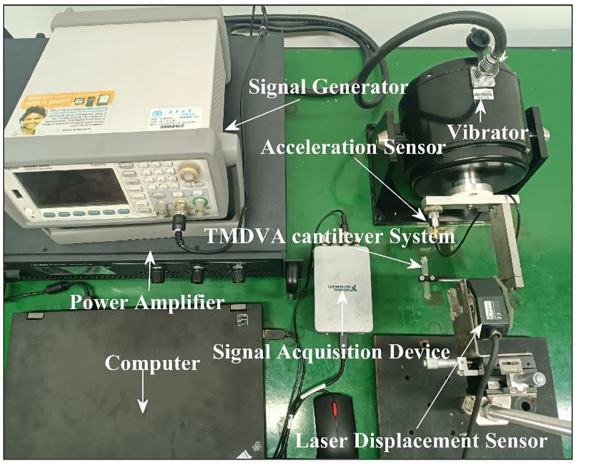

Source(s): Authors' own work

Figure 20.
Experimental dynamic response measurement system

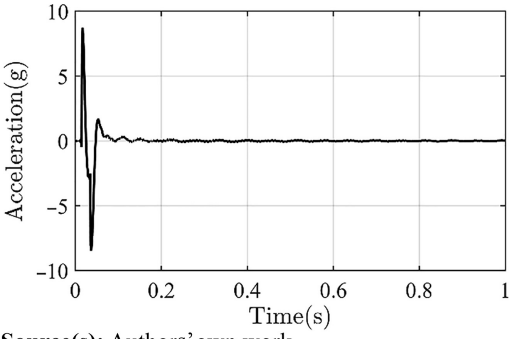

Source(s): Authors' own work

Figure 21.
Experimentally measured excitation acceleration a

leads to its inability to have a strong 1:1 resonance capture with the cantilever with a resonance frequency of 9.5 Hz. In contrast, the TMDVA-48 only lacks stiffness components of less than 7.72 N/m, and it can still exhibit a strong 1:1 internal resonance with the 9.5 Hz cantilever. Based on that, it can also be speculated that when the cantilever's resonance frequency is further reduced, the TMDVA-48 may also fail to achieve strong 1:1 resonance capture due to the lack of stiffness components. The vibration reduction effect of the TMDVA-48 will also be limited as a result.

4. Experiment

In this section, experiments are carried out to verify the correctness of the simulation analysis. First, the nonlinear magnetic force measurement experiments are carried out to check the validity of the F_m calculation model. The parameters of the magnets are shown in Table A1 of Appendix, and the magnet distances are 38 and 48 mm, respectively. Figure 19(a) displays the nonlinear magnetic force measurement system. The measuring range of the dynamometer is [-5 N, 5 N], and the accuracy is 0.001 N. The displacement adjusting knobs are used to adjust the distance s between the magnet B and the magnet A. Meanwhile, the force values acting on the magnet B are recorded.

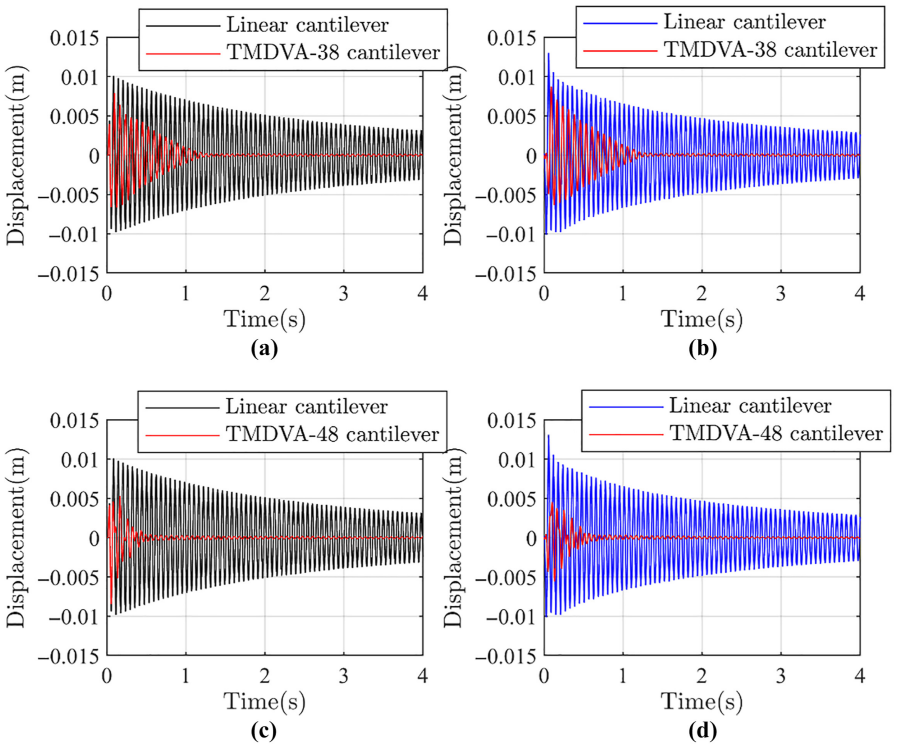

Source(s): Authors' own work

Figure 22. The comparison between the experimental results and simulation results of the cantilever displacement response when the resonance frequency of the linear cantilever is 16.7 Hz. (a) and (c) The simulation results. (b) and (d) The experimental results

Figure 19(b) depicts the comparison of the experimental and theoretical results of the force F_m. And Figure 19(c) is the diagram of the variation of the magnetic force stiffness K_m. The RMSEs are approximately 1.86% (l = 38 mm) and 2.02% (l = 48 mm), respectively. These results indicate that the theoretical results are in good agreement with the experimental data.

Figure 20 shows the experimental dynamic response measurement system. The excitation signal generated by the signal generator **(33500B)** is input into the vibrator through the power amplifier **(LA-200)**, and the vibrator **(MS-200)** excites the TMDVA cantilever vibration reduction system. The acceleration sensor is used for acquiring the excitation acceleration. Then the data can be input into the computer through the signal acquisition device **(NI PXI-1033)**. The sampling frequency of the signal acquisition device is 1.652 kHz. The displacement of the cantilever is measured by the laser displacement sensor **(LK-H050)**, and the data should also be input into the computer. The sampling frequency of the laser displacement sensor is 10 kHz. A triangular pulse signal is generated by the signal generator. The experimentally measured excitation acceleration a is shown in Figure 21, of which the maximum amplitude is 8.7 g. The experimental parameters of the TMDVA and the cantilever are shown in Appendix.

Figure 22 displays the comparison between the experimental results and simulation results of the cantilever displacement response when the resonance frequency of the linear cantilever is 16.7 Hz. The vibration reduction effects of the TMDVA-38 and the TMDVA-48 in the experiment are 63.58% and 78.06%, respectively. Direct measurement of the motion

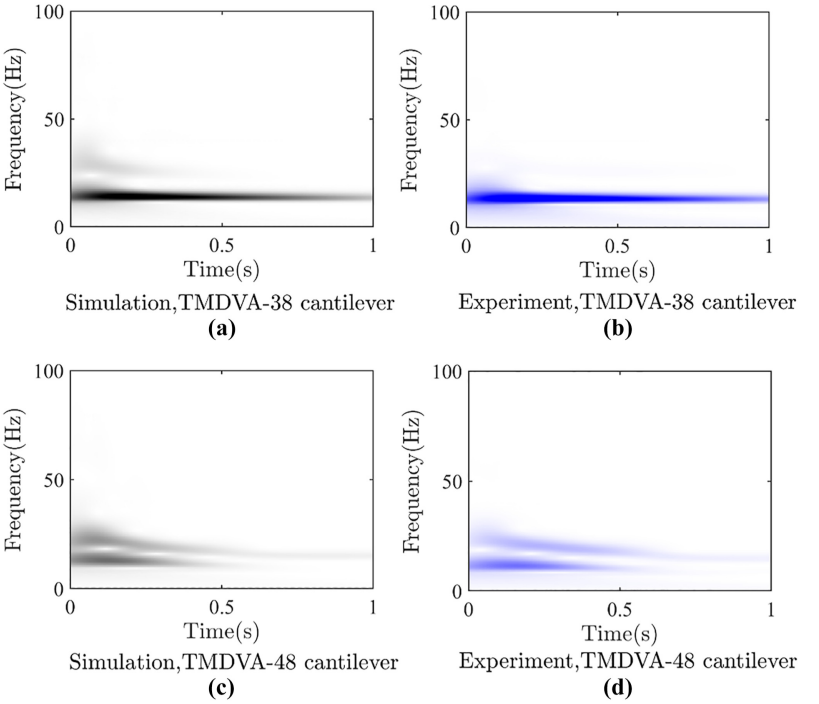

Source(s): Authors' own work

Figure 23.
The WT spectra of the TMDVA cantilever when the resonance frequency of the linear cantilever is 16.7 Hz. (a) and (c) The simulation results. (b) and (d) The experimental results

states of the magnet B cannot be realized given the existing laboratory conditions. However, it can be seen from Section 3 that the motion state of the magnet B will affect the WT spectrum of the cantilever. Therefore, the WT spectrum of the experimental displacement response of the cantilever can be compared with the WT spectrum in the simulation to indirectly verify the motion state of magnet B. Figure 23 shows the experimental and simulation WT spectra of the cantilever displacement response. Figure 23(b) and (d) demonstrate that both the experimental TMDVA-38 and TMDVA-48 show harmonic components consistent with the simulation results, but the super-harmonic resonances in the experimental results are both weaker compared with the simulation results. Particularly, in the TMDVA-38 cantilever system, the energy transfer between the TMDVA-38 and the cantilever relies almost only on the 1:1 internal resonance. This leads to a lower vibration reduction effect of the TMDVA in the experiment than that of the TMDVA in the simulation.

Figure 24 shows the comparison between the experimental results and simulation results of the cantilever displacement response when the resonance frequency of the linear cantilever is 25 Hz. The vibration reduction effects of the TMDVA-38 and the TMDVA-48 in the experiment are 77.18% and 66.53%, respectively. The vibration reduction effect of the TMDVA-38 is better than that of the TMDVA-48. Figure 25 displays the experimental and simulation WT spectra of the cantilever displacement response. The figure illustrates that harmonic components consistent with the simulation results appear in the experimental results. The experimental results are in general agreement with the simulation results. However, Figure 25(b) demonstrates that some subharmonic components also appear in the experimental results of the TMDVA-38 system, which is not obvious in the simulation results

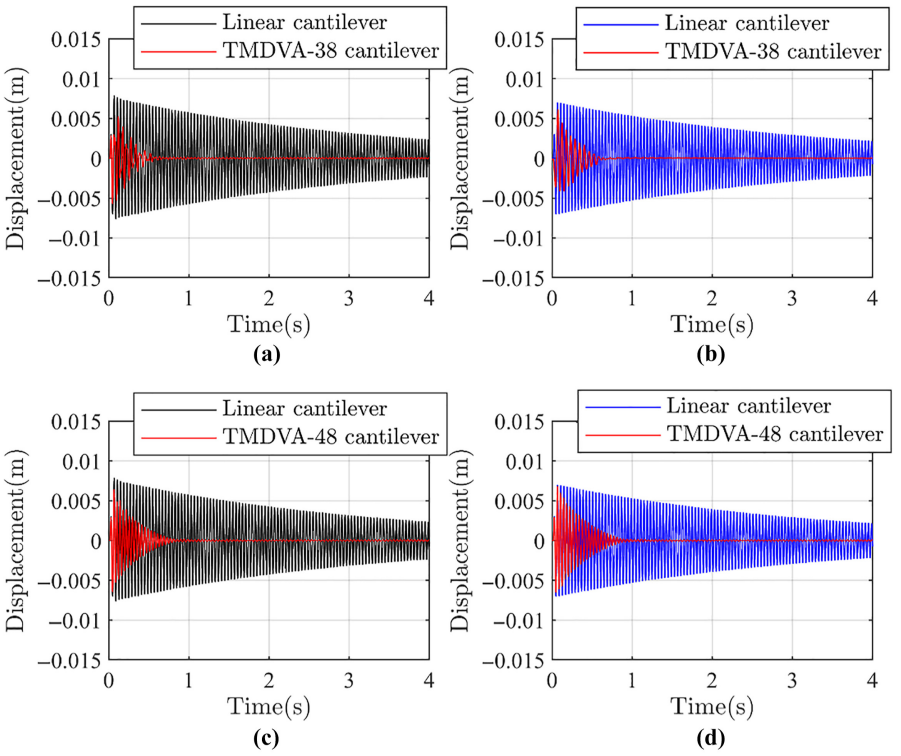

Source(s): Authors' own work

Figure 24. The comparison between the experimental results and simulation results of the cantilever displacement response when the resonance frequency of the linear cantilever is 25 Hz. (a) and (c) The simulation results. (b) and (d) The experimental results

of Figure 25(a). Combined with the WT spectrum of the magnet B in the TMDVA-38 shown in Figure 14(b), it can be found that the subharmonic resonance also appears in the system response of the TMDVA-38 in its simulation analysis. This indicates that the subharmonic resonance appears more strongly in the experimental TMDVA-38 vibration reduction system than in the simulation.

Figure 26 displays the comparison between the experimental results and simulation results of the cantilever displacement response when the resonance frequency of the linear cantilever is 9.5 Hz. The vibration reduction effects of the TMDVA-38 and the TMDVA-48 are 56.25% and 83.03%, respectively. The vibration reduction effect of the TMDVA-48 is better than that of the TMDVA-38 under this condition. Figure 27 depicts the WT spectra of the experimental and simulation displacement response of the cantilever. The figure indicates that when the resonance frequency of the linear cantilever is 9.5 Hz, the harmonic components appear in the experimental results in full agreement with the simulation results.

5. Discussion

Under the parameter conditions of this paper, the simulation and experimental results demonstrate that both the TMDVA-38 and the TMDVA-48 can effectively reduce the vibration of the cantilever, even if the resonance frequency of the cantilever changes. However, the two TMDVAs with different magnet distances show different vibration

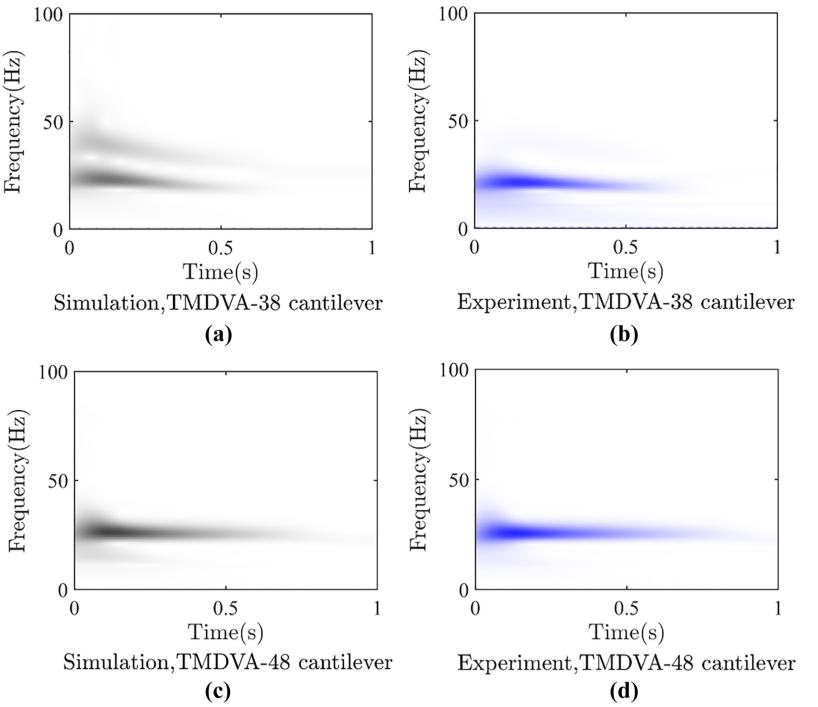

Source(s): Authors' own work

Figure 25.
The WT spectra of the TMDVA cantilever when the resonance frequency of the linear cantilever is 25 Hz. (a) and (c) The simulation results. (b) and (d) The experimental results

reduction performances when the resonance frequency of the cantilever is different. To further investigate the law, under the parameters in Appendix, Figure 28 illustrates the vibration reduction effect of the TMDVA-38 and the TMDVA-48 when the cantilever resonance frequency continuously changes. According to the comparison between Figure 28(a) and (b), it is found that the vibration reduction effect of the TMDVA-38 can reach more than 80% in [24 Hz, 30 Hz], while the vibration reduction effect of the TMDVA-48 can reach more than 80% in [9.5 Hz, 21.5 Hz]. And when the frequency is greater than 22 Hz, the vibration reduction effect of the TMDVA-38 is always better than that of the TMDVA-48. On the contrary, when the frequency is less than 22 Hz, the vibration reduction effect of the TMDVA-48 is better than that of the TMDVA-38. Therefore, the TMDVA-38 is more suitable for vibration reduction in the high-frequency region, while the TMDVA-48 exhibits a better vibration reduction performance in the low-frequency region. As previously mentioned in Section 3, the vibration reduction effect of the TMDVA-38 in the low-frequency region (about less than 10 Hz) is not satisfactory due to the absence of low-stiffness components below 23.63 N/m, while the TMDVA-48 achieves more than 80% vibration reduction effect at 9.5 Hz. Figure 28(b) illustrates that the vibration reduction effect of the TMDVA-48 also decreases rapidly when the resonance frequency of the cantilever is further reduced. Near the frequency of 5 Hz, the vibration reduction effect of the TMDVA-48 is reduced to less than 60%.

Figure 29 displays the vibration reduction effect of the TMDVA with different magnet distance when the resonance frequency of the cantilever changes. This figure shows more comprehensively the relationship between the broadband vibration reduction characteristics of the TMDVA and the magnet distance. The figure clearly indicates that when the resonance

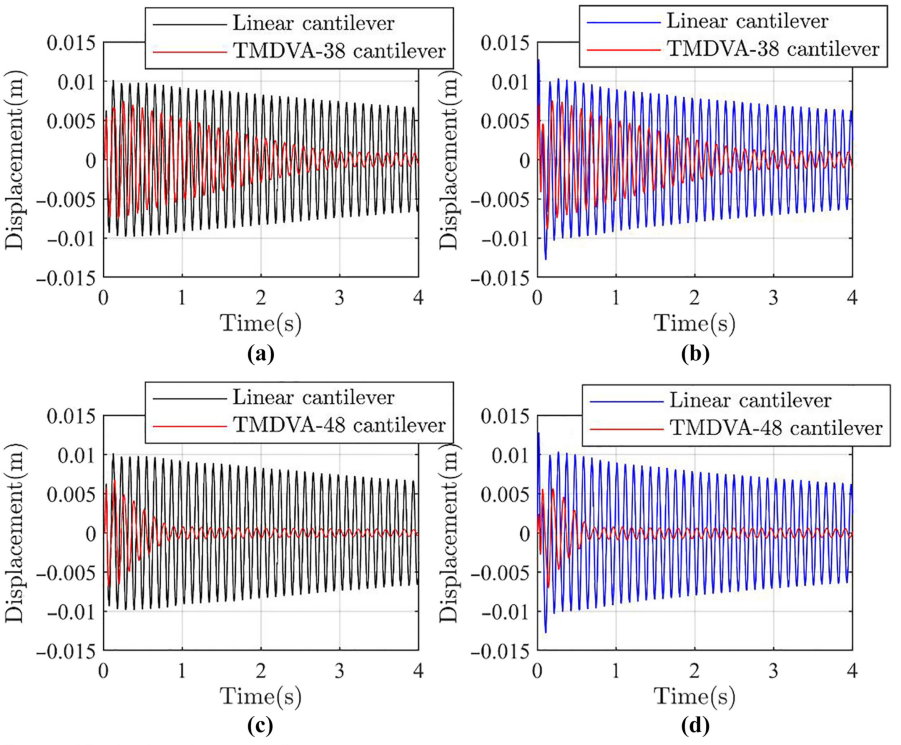

Source(s): Authors' own work

Figure 26.
The comparison between the experimental results and simulation results of the cantilever displacement response when the resonance frequency of the linear cantilever is 9.5 Hz. (a) and (c) The simulation results. (b) and (d) The experimental results

frequency of the cantilever changes, the vibration reduction effect of the TMDVA can reach more than 80% by adjusting the magnet distance properly. Moreover, under such high vibration reduction effects, the figure illustrates that the magnet distance of the TMDVA and the resonance frequency of the cantilever show an approximately linear relationship. That is, to achieve the optimal vibration reduction effect, the higher the resonance frequency of the cantilever, the smaller the magnet distance of the TMDVA. Similarly, the lower the resonance frequency of the cantilever, the larger the magnet distance of the TMDVA. Therefore, for the vibration reduction of the cantilevers with different resonance frequencies, the approximately linear relationship between the magnet distance and the cantilever resonance frequency provides a convenient way to optimize the vibration reduction effect of the TMDVA.

It should be noted that, from Figure 29, when the resonance frequency of the cantilever is close to 5 Hz and the magnet distance is increased to 60 mm, the vibration reduction effect of the TMDVA still cannot reach more than 80%. Moreover, it can be seen from the trend of the image that even if the magnet distance continues to increase, it is too difficult to make the vibration reduction effect of the TMDVA reach more than 80%. This is due to the fact that the effect of the magnet distance on the nonlinear magnetic force characteristics gradually decreases when the magnet distance is larger than a certain value (see Section 2.2.2).

In addition, Figure 29 also demonstrates that when the cantilever resonance frequencies are 9.5 Hz, 16.7 Hz and 25 Hz, respectively, the vibration effect of the TMDVA with magnet

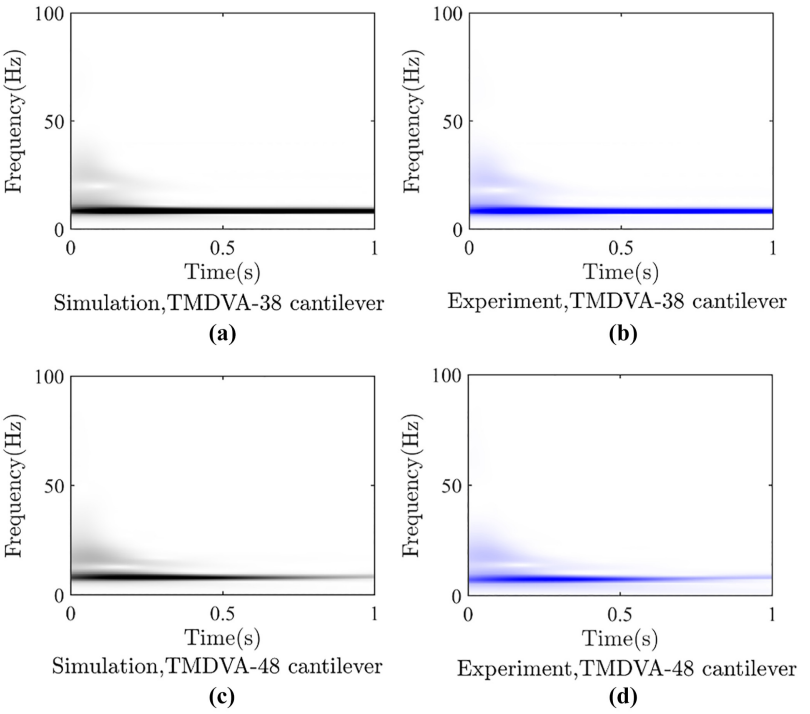

Figure 27.
The WT spectra of the TMDVA cantilever when the resonance frequency of the linear cantilever is 9.5 Hz. (a) and (c) The simulation results. (b) and (d) The experimental results

Source(s): Authors' own work

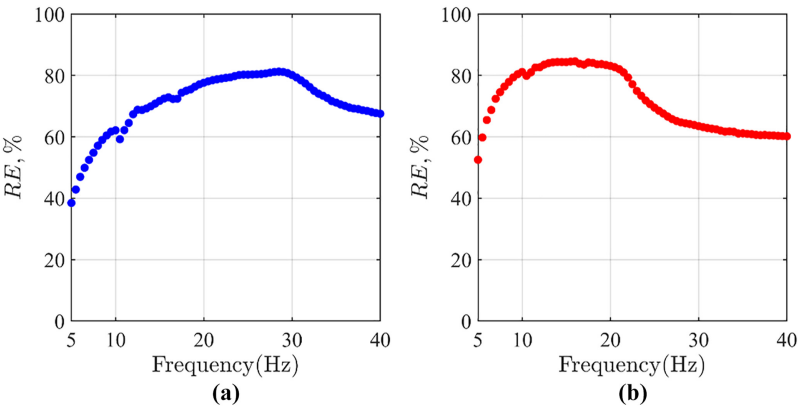

Figure 28.
The vibration reduction effects of (a) the TMDVA-38 and (b) the TMDVA-48 when the resonance frequency changes

Source(s): Authors' own work

distances of 42 mm ~ 60 mm, 36 mm ~ 60 mm and 34 mm ~ 48 mm, respectively, can all reach more than 70%. This illustrates that the TMDVA has strong robustness to magnet distance variations, which reduces the difficulty of selecting or designing the magnet distance for the TMDVA in practical applications.

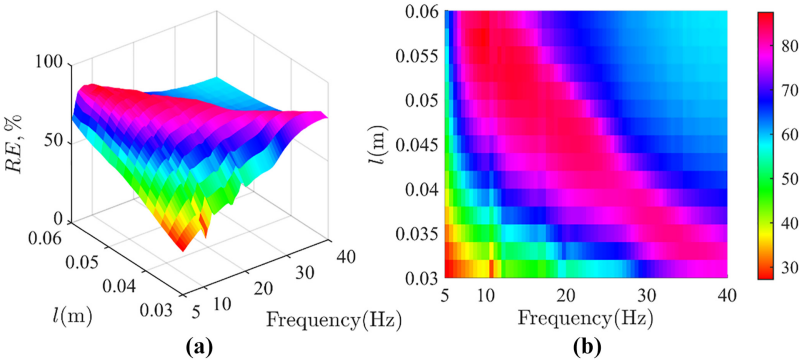

Source(s): Authors' own work

Figure 29. The vibration reduction effect of the TMDVA with different magnet distance when the resonance frequency of the cantilever changes. (a) 3D diagram. (b) Cloud diagram

6. Conclusion

A novel TMDVA with tunable stiffness is designed, modeled and tested. The tuning methodology is passive and the adjustment of the TMDVA's stiffness can be achieved by changing the magnet distance of the TMDVA. With its simple structure, the TMDVA is easy to be implemented and miniaturized. The magnet distance of the TMDVA affects the nonlinear magnetic stiffness characteristics, and ultimately affects the vibration reduction performance of the TMDVA. Therefore, the vibration reduction effect of the TMDVA can be optimized by adjusting the magnet distance. When the resonance frequency of the cantilever is different, the magnet distance of the TMDVA with a high vibration reduction effect shows an approximately linear relationship with the resonance frequency of the cantilever, which is convenient for the design optimization of the TMDVA. Taken together, the TMDVA, with strong robustness, can effectively reduce the vibration of the cantilever even if the resonance frequency of the cantilever changes. The TMDVA has potential application value in the vibration reduction of engineering structures.

References

Bae, J.S., Hwang, J.H., Roh, J.H., Kim, J.H., Yi, M.S. and Lim, J.H. (2012), "Vibration suppression of a cantilever beam using magnetically tuned-mass-damper", *Journal of Sound and Vibration*, Vol. 331, pp. 5669-5684.

Benacchio, S., Malher, A., Boisson, J. and Touze, C. (2016), "Design of a magnetic vibration absorber with tunable stiffnesses", *Nonlinear Dynamics*, Vol. 85, pp. 893-911.

Chen, Y., Qian, Z., Zhao, W. and Chang, C. (2020), "A magnetic Bi-stable nonlinear energy sink for structural seismic control", *Journal of Sound and Vibration*, Vol. 473, 115233.

Chen, X., Leng, Y., Sun, F., Su, X., Sun, S. and Xu, J. (2023a), "A novel triple-magnet magnetic suspension dynamic vibration absorber", *Journal of Sound and Vibration*, Vol. 546, 117483.

Chen, X., Leng, Y., Sun, F., Su, X., Sun, S. and Xu, J. (2023b), "Design and modeling of a novel triple-magnet magnetic dynamic vibration absorber", *International Journal of Applied Electromagnetics and Mechanics*, Vol. 71 No. 4, pp. 363-388.

Chen, X., Leng, Y., Sun, F., Su, X., Sun, S. and Xu, J. (2023c), "Passive vibration reduction performance of a triple-magnet magnetic suspension dynamic vibration absorber under sinusoidal excitation", *Acta Mechanica Sinica*, Vol. 39, 522286.

Cheng, Z., Antonio, P., Shi, Z. and Marzani, A. (2020), "Enhanced tuned mass damper using an inertial amplification mechanism", *Journal of Sound and Vibration*, Vol. 475, 115267.

Christie, M.D., Sun, S., Deng, L., Ning, D.H., Du, H., Zhang, S.W. and Li, W.H. (2019), "A variable resonance magnetorheological-fluid-based pendulum tuned mass damper for seismic vibration suppression", *Mechanical Systems and Signal Processing*, Vol. 116, pp. 530-544.

Den Hartog, J.P. (1947), *Mechanical Vibrations*, pp. 112-132, McGraw-Hall Book Company, New York.

Di Matteo, A., Masnata, C. and Pirrotta, A. (2019), "Simplified analytical solution for the optimal design of tuned mass damper inerter for base isolated structures", *Mechanical Systems and Signal Processing*, Vol. 134, 106337.

Geng, X., Ding, H., Mao, X. and Chen, L. (2021), "Nonlinear energy sink with limited vibration amplitude", *Mechanical Systems and Signal Processing*, Vol. 156, 107625.

Gourdon, E., Alexander, N.A., Taylor, C.A., Lamarque, C.H. and Pernot, S. (2007), "Nonlinear energy pumping under transient forcing with strongly nonlinear coupling: theoretical and experimental results", *Journal of Sound and Vibration*, Vol. 300, pp. 522-551.

Guo, C., AL-Shudeifat, M.A., Vakakis, A.F., Bergman, L.A., McFarland, D.M. and Yan, J. (2015), "Vibration reduction in unbalanced hollow rotor systems with nonlinear energy sinks", *Nonlinear Dynamics*, Vol. 79, pp. 527-538.

Housner, G.W., Bergman, L.A., Caughey, T.K., Chassiakos, A.G., Claus, R.O., Masri, S.F., Skelton, R.E., Soong, T.T., Spencer, B.F. and Yao, J.T.P. (1997), "Structural control: past present, and future", *Journal of Engineering Mechanics ASCE*, Vol. 123, pp. 897-971.

Javidialesaadi, A. and Wierschem, N.E. (2019), "An inerter-enhanced nonlinear energy sink", *Mechanical Systems and Signal Processing*, Vol. 129, pp. 449-454.

Liu, Y., Yu, D., Zhao, H. and Wen, X. (2007), "Review of passive dynamic vibration absorbers", *Journal of Mechanical Engineering*, Vol. 43, pp. 14-21.

Lo Feudo, S., Touzé b, C., Boisson, J. and Cumunel, G. (2019), "Nonlinear magnetic vibration absorber for passive control of a multi–storey structure", *Journal of Sound and Vibration*, Vol. 438, pp. 33-53.

Ormondroyd, J. and Den Hartog, J.P. (1928), "The theory of the dynamic vibration absorber", *Journal of Applied Mechanics*, Vol. 50, pp. 9-22.

Oueini, S.S., Chin, C.M. and Nayfeh, A.H. (1999), "Dynamics of a cubic nonlinear vibration absorber", *Nonlinear Dyn*, Vol. 20, pp. 283-295.

Pennisi, G., Mann, B.P., Naclerio, N., Stephan, C. and Michon, G. (2018), "Design and experimental study of a Nonlinear Energy Sink coupled to an electromagnetic energy harvester", *Journal of Sound and Vibration*, Vol. 437, pp. 340-357.

Priya, S., Inman, D.J., Translated by, Huang, J.Q. and Huang, Q.A. (2010), *Energy Harvesting Technologies*, Southeast University Press, Nanjing, pp. 1-4.

Pun, D. and Liu, Y.B. (2000), "On the design of the piecewise linear vibration absorber", *Nonlinear Dynamics*, Vol. 22, pp. 393-413.

Roberson, R.E. (1952), "Synthesis of a nonlinear dynamic vibration absorber", *Journal of the Franklin Institute*, Vol. 254, pp. 205-220.

Tripathi, A., Grover, P. and Kalmár-Nagy, T. (2017), "On optimal performance of nonlinear energy sinks in multiple-degree-of-freedom systems", *Journal of Sound and Vibration*, Vol. 388, pp. 272-297.

Vakakis, A.F. (2001), "Inducing passive nonlinear energy sinks in vibrating systems", *Journal of Vibration and Acoustics*, Vol. 123, pp. 324-332.

Vakakis, A.F., Gendelman, O.V., Bergman, L.A., Mcfarland, D.M., Kerschen, G. and Lee, Y.S. (2008), *Nonlinear Targeted Energy Transfer in Mechanical and Structural Systems*, Springer-Verlag, New York, pp. 310-336.

Walsh, P.L. and Lamancusa, J.S. (1992), "A variable stiffness vibration absorber for minimization of transient vibrations", *Journal of Sound and Vibration*, Vol. 158, pp. 195-211.

Xu, J. (2015), "Advances of research on vibration control", *Chinese Quarterly of Mechanics*, Vol. 36, pp. 547-565.

Yao, J.T.P. (1972), "Concept of structural control", *Journal of the Structural Division*, Vol. 98, pp. 1567-1574.

Yao, H., Cao, Y., Ding, Z. and Wen, B. (2019), "Using grounded nonlinear energy sinks to suppress lateral vibration in rotor systems", *Mechanical Systems and Signal Processing*, Vol. 124, pp. 237-253.

Zhang, Y. and Leng, Y. (2020), "Special behaviors of two interacting permanent magnets with large different sizes", *International Journal of Applied Electromagnetics and Mechanics*, Vol. 62, pp. 315-329.

Zhang, Y., Leng, Y., Tan, D., Liu, J. and Fan, S. (2017), "Accurate analysis of magnetic force of bi-stable cantilever vibration energy harvesting system with the theory of magnetizing current", *Acta Physica Sinica*, Vol. 66, pp. 154-166.

Zhang, Y., Lu, Y. and Chen, M.L. (2019), "Energy harvesting via nonlinear energy sink for whole - spacecraft", *Science China Technological Sciences*, Vol. 62, pp. 1483-1491.

Zhang, Y., Leng, Y., Zhang, H., Su, X., Sun, S., Chen, X. and Xu, J. (2020), "Comparative study on equivalent models calculating magnetic force between permanent magnets", *Journal of Intelligent Manufacturing and Special Equipment*, Vol. 1 No. 1, pp. 43-65.

Appendix

Material	Parameter	Numerical value
Magnet B material	Density ρ_B/ kg·m^{-3}	7,500
$Nd_2Fe_{14}B$ (N42)	Height l_B/ mm radius r_B/ mm	9.95
	Magnetization M_B/ A·m^{-1}	2.985
		7.4×10^5
Magnet A and C material	Density ρ_A/ kg·m^{-3}	7,500
$Nd_2Fe_{14}B$ (N42)	Height l_A/ mm radius r_A/ mm	4
	Magnetization M_A/ A·m^{-1}	2.985
	Vacuum permeability μ_0/ N·A^{-2}	$7.4 \times 10^5 4\pi \times 10^{-7}$

Source(s): Authors' own work

Table A1. Parameters of magnets A, B and C

Material	Parameter	Numerical value
Cantilever beam E: Silicon steel	Young's modulus E/ GPa	200
	Density ρ_c/ kg·m^{-3}	7,700
	Length l_c/ mm	52/92/140
	Width w_c/ mm	10.02
	Height t_c/ mm	0.55
	Damping ratio ξ_r	0.0021
Magnetic suspension tube D: Acrylic plastic	Density ρ_g/ kg·m^{-3}	1,200
	Length l_g/ mm	58
	Inner radius r_i/ mm	3.05
	Outer radius r_o/ mm	4.01
	Friction coefficient μ	0.3
	Damping coefficient c_2/N/m	0.02
Gripper G: Acrylonitrile Butadiene Styrene copolymers (ABS)	Mass/kg	0.0029

Source(s): Authors' own work

Table A2. Parameters of the cantilever system

Corresponding author
Yonggang Leng can be contacted at: leng_yg@tju.edu.cn